Ultrasonics 94 (2019) 192–201

Contents lists available at ScienceDirect

Ultrasonics

journal homepage: www.elsevier.com/locate/ultras

Structures and dynamics of carbon-black in suspension probed by static and dynamic ultrasound scattering techniques

Motoki Ozaki, Tomohisa Norisuye*, Hideyuki Nakanishi, Qui Tran-Cong-Miyata

Department of Macromolecular Science and Engineering, Graduate School of Science & Technology, Kyoto Institute of Technology Matsugasaki, Sakyo-ku, Kyoto 606-8585, Japan

A B S T R A C T

Carbon black (CB) suspension exhibits various structures depending on the properties of solvent and dispersant as well as the preparation process of suspension. In most cases, CB particles do not exist as independent nanoparticles but as aggregates or agglomerates. In order to evaluate the size distribution at different level of hierarchal structure, we carried out static/dynamic ultrasound scattering analysis for the CB suspensions in alcohol and/or water with or without Nafion, a perfluorinated polymer. The potential of the dynamic ultrasound scattering technique was demonstrated by discriminating diffusing nanoparticles and micron-sized aggregates/agglomerates without dilution of the sample. Particularly, suppression of large agglomerates by addition of Nafion was clearly observed. Phosphotungstic acid (PWA), a family of polyoxometalate, was also employed to obtain smaller unit structures of the CB particles without formation of aggregation after decomposition of CB. The possible structures of the CB/PWA suspensions with and without Nafion were also discussed.

1. Introduction

Carbon black (CB) is widely used as black pigment [1], reinforcing agent [2], and platinum-catalyst supports for fuel cell [3]. It is obtained by pyrolysis of hydrocarbon [4], graphitization of polypyrrole nanoparticles during carbonization [5], or electrolysis in molten alkali halide salts [6]. Polyoxometalates are known as an effective stabilizer to obtain nano-sized carbon particles from large carbon aggregates by decomposition under sonication [7]. In general, the CB suspension is prepared by dispersing CB in a polar solvent, such as water, alcohol, or their mixture, with an appropriate surfactant or a polymer dispersant. Surface modification was also attempted to improve the dispersibility of carbon black particles at desired pH [8–10]. Since the performance of the product, e.g., the electro-conductivity or mechanical properties, is considered to be dependent on the hierarchal structures of carbon-black particles [11,12], developing techniques to evaluate the structures and properties without dilution or drying is highly demanded.

The primary size of carbon-black particle in suspension ranges from several tens of nanometers to several hundreds of nanometers. Studies by transmission electron microscopy with high resolution revealed that the internal structure of carbon particles consisted of bent subunits or single bent graphene layers depending on the processing method [13]. A concentric structure of graphene layers inside the particle is composed of assembly of hexagonal, pentagonal, and heptagonal rings, in which the pentagonal and heptagonal rings are respectively responsible for the positive and negative curvatures of the graphitic flakes [14]. These primary particles are developed to form aggregates [15], or weakly-bonded agglomerates in suspensions [16].

In order to control the quality of the product, as mentioned above, it is crucial to understand the size distribution of primary particle, aggregation and its agglomerate in suspension. It should be noted that the measurement must be carried out in-situ without dilution or drying because the structures of particles could be different from those of original suspension once it is diluted. At this point, dynamic techniques are good candidates to provide particle size distribution as well as the interactions between particles in liquid. Zeta potential is also employed to evaluate the surface charge of particle [17]. Compared to the static techniques providing visual images or time-averaged spectra, such as electron microscope, x-ray and neutron scattering methods, dynamic measurements offer rich information on the particle environment via the time-dependence of the particle position. For example, the time-correlation function approach allows us to distinguish different particle dynamics, e.g., thermal fluctuations of nano-particles (random motion), electrophoretic motion of charged particles, sedimentation of large aggregates or agglomerates (ballistic motion). While the dynamic light scattering (DLS), diffusing wave spectroscopy (DWS) and low-coherence DLS method could be an effective tool to investigate suspensions, optically non-transparent suspensions such as carbon black inks must be more or less diluted to allow transmission of light source.

So far, we have developed a novel ultrasound technique called high-frequency dynamic ultrasound scattering (DSS) [18]. The technique is an acoustic analog of DLS, which can be used to investigate the particle

* Corresponding author.
E-mail address: nori@kit.jp (T. Norisuye).

https://doi.org/10.1016/j.ultras.2018.09.012
Received 30 March 2018; Received in revised form 24 September 2018; Accepted 24 September 2018
Available online 29 September 2018
0041-624X/

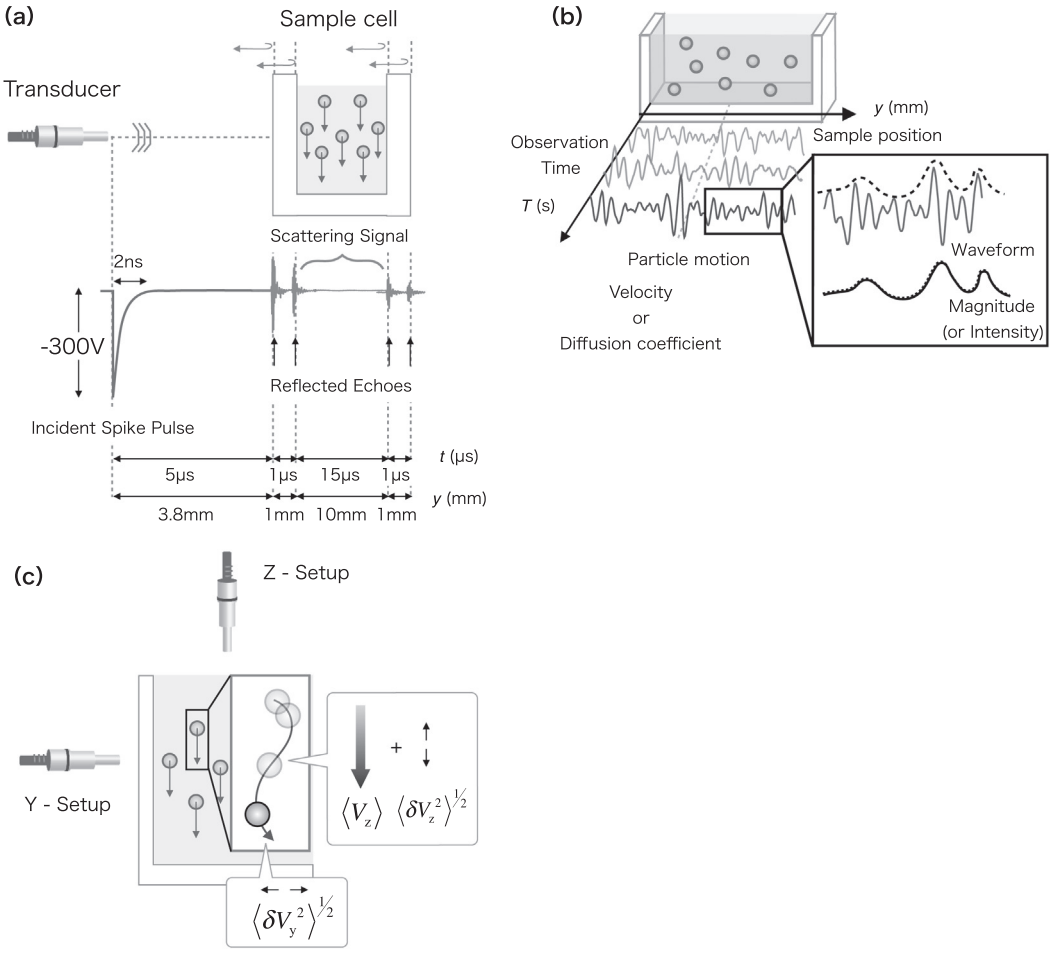

Fig. 1. Schematic representations of (a) the sample cell and the waveform. (b) The time evolution of the scattered field profile and (c) the experimental setup along the direction of sedimentation (Z-Setup) and perpendicular to sedimentation (Y-Setup).

motion in liquid [19]. Although the wavelength of ultrasound is relatively long compared to visible light, particle sizing down to several tens of nanometers using 30 MHz longitudinal ultrasound has recently achieved [20]. The phase-mode DSS technique also allows us to visualize the spatiotemporal information on the particle motion [21,22]. All these techniques are useful to investigate the particle suspension accompanying small and large aggregates. The frequency-domain dynamic ultrasound scattering (FD-DSS) technique revealed that the dynamics of aqueous suspension of submicron silica particles accompanied hydrodynamic velocity fluctuations in addition to Brownian motion. Since the mean-squared displacement evaluated by the FD-DSS technique showed different time-dependence [20,23], the technique could be employed to discriminate the primary particles, secondary aggregates, and ternary agglomerate of carbon-black particles in suspension without dilution of the sample. In this study, we demonstrate the potential of the FD-DSS technique by showing the dynamics of carbon black suspension with or without Nafion, a perfluorinated polymer dispersant.

2. Experimental procedure

50% compressed acetylene carbon black (CB) was purchased from Sterm Chemical (USA). The CB particles were dispersed in a solvent with or without Nafion as a dispersant under sonication. Two types of Nafion solutions, DE521 and DE1021, were purchased from Wako Chemical, JAPAN. For DE521, Nafion was dissolved in a mixed solvent to form the mixture of Nafion: water: 1-propanol with the ratio 5: 45: 50. DE1021 is an aqueous solution containing 10% of Nafion without alcohol. Hereafter, the suspension of CB particles dispersed in DE521 is regarded as an alcohol-rich system, while those in DE1021 can be considered as a water-rich system. The CB concentration was varied in range 0.3–1.0 wt%.

The density of particles was determined by the density matching method with calibrated aqueous solutions of sodium polytungstate, SPT ($3Na_2WO_4{\cdot}9WO_3{\cdot}H_2O$). The density of the SPT solution was calibrated using a 25 mL Gay-Lussac pycnometer prior to the density matching experiments. The density of carbon black was determined to be 1.84 (g/cm^3), which is closer to the values reported in literatures [24,25].

Field-Emission Scanning Electron Microscope (FE-SEM; JEOL JSM-7600F) images were taken to verify the particle size and its distribution. The obtained bitmap images were recorded with 2560 × 1920 pixels containing about 10 particles in each picture, followed by the calculation of the diameter.

A water-immersion longitudinal wave transducer having a nominal central frequency of 30 MHz (30K1I, KGK Japan) was employed in the dynamic ultrasound scattering experiments. Typical waveform amplitude was 1 V peak-to-peak with the 0.4 μs pulse duration. The standard deviation of the white noise level was found to be 140 μV. The main frequency was found to be 32 MHz after calibration of the transducer by the method provided in the previous paper [26]. The corresponding wavelength in water is about 50 μm. The energy of pulser as well as the pulse repetition frequency was kept as low as possible to avoid unexpected flow induced by excess ultrasound energy (or acoustic radiation force) [27]. The transducer and the cell container were carefully aligned using a custom-made stainless stage coupled with rotational (α, β and γ) and translational (x, y, z) stages prior to the back scattering

experiments in order to avoid the signal loss originated from misalignment with respect to the cell wall where α, β and γ were the axially tilting angle in the yz, zx, and xy planes, respectively. Disposable polystyrene rectangular vessels with the dimension $10 \times 10 \times 40\,mm^3$ and the wall thickness 1 mm were used as the sample cells. The signal was recorded by a 14-bit high-speed digitizer, GaGe CS-14200, with the sampling rate 200 Mega samples/s. All the digital devices were synchronized with a 10 MHz reference clock to avoid phase jittering. The sample was set in a homemade thermostat bath regulated at 25 ± 0.01 °C.

3. Ultrasound scattering analysis

When an ultrasound pulse wave generated by a negative spike pulser equipped with an ultrasonic transducer is irradiated onto the sample cell containing a particle suspension, one observes, as a response, four reflected echoes from the cell walls. The horizontal (Y) experimental setup and the corresponding waveform were represented in Fig. 1(a) where t denotes the pulse propagation time. For particle suspensions, one may observe scattering signals between the two sample cell walls. Such scattering signals are repetitively (typically 20,000 times) recorded at a constant time interval (the time repetition time, ΔT, typically 50–300 ms) of during the particle motion. The time-evolution of the scattering pulse field is schematically illustrated in Fig. 1(b). The instantaneous velocity or the diffusion coefficient is evaluated from the observation time T dependence of the scattered amplitude or the corresponding intensity at a depth inside the cell. In this back scattering geometry, the direction of the scattering wave vector coincides with the pulse propagation direction so that the ultrasound scattering experiments with the Y - setup provide information on the horizontal fluctuation of the particle motion. On the other hand, when an ultrasound pulse impinges along the vertical (Z) direction as shown in Fig. 1(c), the particle motion along the sedimentation direction is observed. In this vertical setup, the vertical component of the fluctuation $\langle \delta V_z^2 \rangle_T^{\frac{1}{2}}$ as well as the non-zero component of the average sedimentation velocity $\langle V_z(t) \rangle_T$ can be detected where the bracket indicate the observation time average, and the instantaneous velocity is denoted by $V_z(t, T) = \langle V_z(t) \rangle_T + \delta V_z(t, T)$ as a function of the observation time, T, at a fixed propagation time window, t. Note that the above Y - setup probes the dynamics perpendicular to the sedimentation direction. Therefore, the horizontal fluctuation component $\langle \delta V_y^2 \rangle_T^{\frac{1}{2}}$ is solely obtained without contribution from the average velocity. The pulse propagation time t can be converted into the depth inside the cell $y = ct/2$ by evaluating the product of sound velocity c and round-trip propagation time $t/2$.

Besides the time-domain dynamic ultrasound scattering (TD-DSS) technique, the frequency-domain dynamic ultrasound scattering (FD-DSS) technique gives better insight about the length-scale dependent dynamics [20,26]. Briefly, FD-DSS analysis is performed by taking Fourier transformation of the scattered pulse field in order to decompose the signal into individual frequency components, followed by evaluation of the time-correlation function of the temporal amplitude at a fixed frequency, f. After carrying out similar analysis for all the frequencies, the decay curve with different frequency contributions could be obtained. The 30K1I-broadband transducer covers the frequency range from 27 MHz to 32 MHz. In our previous study, we showed that the particle motion associated with the short-range Brownian motion was detected at relatively high frequency, while from the low frequency regime, the dynamics accompanying long-range hydrodynamic interactions associated with the sedimentation velocity fluctuation was observed [23]. Such information is inaccessible by the conventional TD-DSS. In this study, the FD-DSS technique will be employed to explore the particle motion of the carbon black suspensions.

Ultrasonic spectroscopy was employed to investigate the rigidity of aggregates, and to ensure the discussion of particle sizing. The attenuation coefficient and the phase velocity were analyzed using the relations,

$$\alpha(f) = -\frac{2}{L}\left\{\ln \frac{A_{sam}(f)}{A_{ref}(f)}\right\} + \alpha_{ref}(f), \tag{1}$$

$$c(f) = \frac{2\pi f L}{\theta_{sam}(f) - \theta_{ref}(f) + \frac{2\pi f L}{c_{ref}(f)} + 2m\pi}, \tag{2}$$

where L is the sample size, A is the amplitude and θ is the phase of the transmitted pulse,"sam" and "ref" respectively refer to the sample and reference. Evaluation of the appropriate number of m, is described elsewhere [28]. The transmission loss due to mismatch of the acoustic impedance between the sample and the cell wall is negligibly small for our case. The theoretical values of α and c for particle suspensions were calculated using the real and imaginary part of the effective wavenumber k given by,

$$k = \frac{2\pi f}{c} + i\frac{\alpha}{2} \tag{3}$$

The single particle scattering function $F(\Theta)$ at the angle Θ, and the effective wavenumber are related by the dispersion relation [29–31].

$$\left(\frac{k}{k_0}\right)^2 = 1 + \sum_j \left\{ \frac{4\pi N_j(d_j) F_j(0)}{k_0^2} - \frac{4\pi^2 N_j^2(d_j)}{k_0^4} \left[F^2(0) - F^2(\pi) + \int_0^\pi \frac{1}{\sin(\Theta/2)} \frac{d}{d\Theta} F^2(\Theta) d\Theta \right] \right\}, \tag{4}$$

was employed in order to reproduce the acoustic properties at finite concentrations where $N_j(d_j)$ is the number concentration of particle with the diameter d_j for the jth particle, k_0 is the complex wavenumber for the reference given by

$$k_0 = \frac{2\pi f}{c_{ref}} + i\frac{\alpha_{ref}}{2} \tag{5}$$

The method to evaluate the $F(\Theta)$ is described in the previous paper [32]. In this paper, the scattering function theory proposed by Epstein-Carhart-Allegra-Hawley (so called the ECAH theory [33–36]) without the thermal contribution was employed.

4. Results and discussions

First, we carried out the DSS analysis of the CB suspensions in the absence of Nafion to investigate the size distribution of CB without any dispersant. Fig. 2(a) shows a two-dimensional image of the scattering intensity obtained for the water-rich CB suspensions at 0.3 wt% without Nafion where the left and bottom axes respectively indicate the pulse propagation time, t, and observation time, T. Since ultrasound pulse was irradiated along the vertical (Z-) direction in this experiment, the depth profile of the particle motion can be acquired as a function of T. The noticeable scatterers, presumably originated from the large agglomerates, were found during observation, then, slowly passed through the scattering volume. Similar large scatterers were also found in the data acquired from 10 different runs as demonstrated in Fig. 1(c)–(e). Since the pulse propagation time, t, multiplied by the sound speed of suspension, c, can be converted into the corresponding round-trip distance, $2z$, the sedimentation velocity of the slowly settling object is estimated by the z-T slope of the image. From the settling velocity, the size of the settling object could be determined using the relation,

$$\langle V_z \rangle_T = V_0(1-\phi)^\nu = \frac{2a^2 \Delta\rho g}{9\eta}(1-\phi)^\nu, \tag{6}$$

where $\langle V_z \rangle_T$ is the average velocity of the settling object, ϕ is the total volume fraction of the CB particle, a is the particle radius, $\Delta\rho = 0.84$ (g/cm^3) is the density difference between the CB particles and water, g

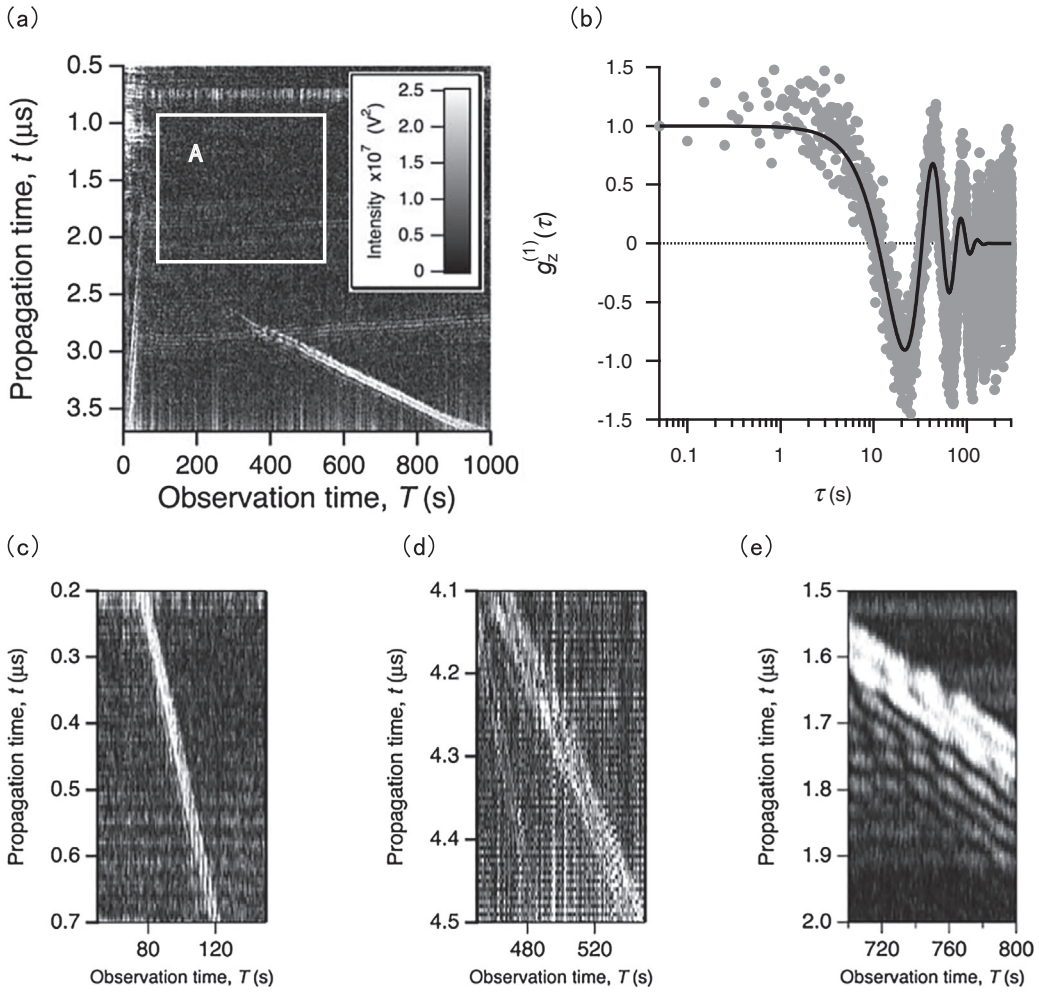

Fig. 2. (a), (c)–(e) examples of two-dimensional image of the scattered intensity obtained for the water-rich CB suspensions at 0.3 wt% without Nafion. (b) An example of the correlation function extracted from the solid square region A in the image (a).

is gravitational acceleration, $\eta = 0.892$ (mPa·S) is the viscosity of water, and ν is the appropriate exponent for the Richardson-Zaki law [37]. Typical particle radius obtained by the analysis was 0.4–2 μm. The correlation function approach also gives information on the dynamics of particles. For example, as indicated by the solid square A in Fig. 2(a), the field time-correlation function, $g^{(1)}(\tau)$, can be constructed from the region of interest. An example of the correlation function extracted at 29.7 MHz is depicted in Fig. 2(b). The time-correlation function, which probes the dynamics along the sedimentation direction Z, involves a sinusoidal oscillation with an exponential decay. The oscillation and the decay respectively give the average settling velocity and the standard deviation (velocity fluctuations). The correlation function may be expressed by [38],

$$g_z^{(1)}(\tau) = \cos(q\langle V_z\rangle_T \tau)\exp\left(-\frac{1}{2}q^2\langle \delta V_z^2\rangle_T \tau^2\right) \tag{7}$$

By fitting the data to above equation, the average sedimentation velocity $\langle V_z\rangle_T$ and its standard deviation (velocity fluctuation) $\langle \delta V_z^2\rangle_T^{\frac{1}{2}}$ are respectively evaluated to be 5.7×10^{-4} (mm/s), and 8.0×10^{-5} (mm/s), which gives average particle radius of 503 nm. The correlation function was evaluated from relatively homogeneous area in the image. Nevertheless, the size of scatterer was found to be in submicron regime. From the analysis, it was found that the aqueous suspension without Nafion was fairly heterogeneous containing large aggregates or agglomerates. Note that, compared to the slowly falling (strong intensity) object found in Fig. 2(a), the submicron/micron-sized particle evaluated by the correlation function showed weaker scattered intensity and smaller velocity. Hereafter, we call the strong intensity object found in the Fig. 2(a) as ternary agglomerate, and the submicron/micron-sized object evaluated by the correlation function from the homogenous area (solid square A) as secondary aggregates. In this image, no primary nanoparticle was found, and they tended to form aggregates.

As described above, the Y-setup (perpendicular to sedimentation) allows us to solely investigate the velocity fluctuation of the CB suspension without average sedimentation component, i.e., the time-correlation function decays exponentially without sinusoidal oscillation. This is particularly useful to discriminate the type of fluctuation from the time exponent of the mean square displacement $\langle r^2\rangle \sim \tau^n$ (e.g., thermal diffusion of nanoparticle is $\langle r^2\rangle = 2D\tau \sim \tau^1$, and micron-particle sedimentation accompanying strong hydrodynamic fluctuations is $\langle r^2\rangle = \langle \delta V_y^2\rangle \tau^2 \sim \tau^2$). Fig. 3(a) shows the time-correlation function obtained for the 0.3 wt% CB aqueous suspension without Nafion observed from the Y-setup. The double logarithmic plot of $\ln g^{(1)}(t)$ indicated that sedimentation accompanying the velocity fluctuations ($n = 2$) as shown in the inset of Fig. 3(a). The correlation function for micron-sized objects observed by the Y-setup may be expressed by,

$$\begin{aligned} g_y^{(1)}(t,\tau) &= \exp\left(-\tfrac{1}{2}q^2\langle r^2\rangle\right) \\ &= \exp\left(-\tfrac{1}{2}q^2\langle \delta V_y^2\rangle_T \tau^2\right) \end{aligned} \tag{8}$$

The curve fitting with the equation gave the standard deviation of

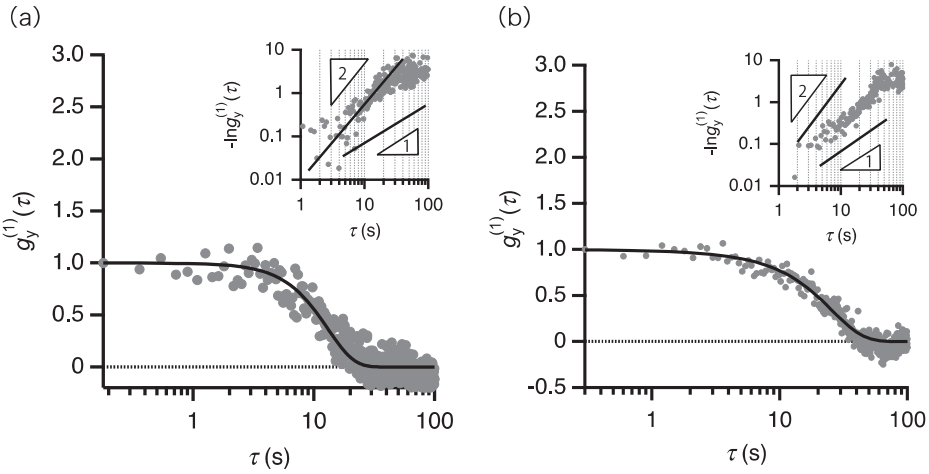

Fig. 3. (a) The time-correlation function obtained for the 0.3 wt% CB aqueous suspension without Nafion observed from the horizontal (Y-) direction. The inset shows the double logarithmic plot of $-\ln g^{(1)}(\tau)$. (b) The time-correlation function after 3 h.

the velocity $\langle \delta V_y^2 \rangle_T^{\frac{1}{2}} = 3.74 \times 10^{-4}$ (mm/s). According to the theory of velocity fluctuations [38–42], $\langle \delta V_y^2 \rangle_T^{\frac{1}{2}}$ may be given by,

$$\langle \delta V_y^2 \rangle_T^{\frac{1}{2}} = C_y V_0 \sqrt{\frac{\phi L}{a}} \tag{9}$$

where C_y is a proportional constant, L is the smallest cell dimension. Although the equation indicates that the particle sizing is possible with known parameters, we will not explore the analysis further since the constant C_y for the CB particle is unknown here. But as for trial analysis, $C_y = 0.1$ gave $a = 755$ nm. When the sample is aged for 3 h, the larger aggregates settled down and the smaller particles remained in supernatant of the sample. As shown in Fig. 3(b), the relaxation time became longer. Although the larger particles were disappeared from the scattering volume, the time exponent n of the correlation function was 1.5 (not unity). This indicates that the particles dynamics is still dominated by non-Brownian motion, which is characteristic for submicron to micron-sized objects [20]. By fitting the data to a cross-over model function with the two adjustable parameters D and $\langle \delta V_y^2 \rangle_T^{\frac{1}{2}}$ proposed in the paper,

$$g_y^{(1)}(\tau) = \exp(-Dq^2\tau) \exp\left(-\frac{1}{2} q^2 \langle \delta V_y^2 \rangle_T \tau^2\right), \tag{10}$$

which takes both diffusive and sedimentation modes into account, one obtains the diffusion coefficient, D. D can be further converted to the hydrodynamic radius via so-called the Stokes-Einstein relation,

$$D = \frac{k_B T}{6\pi\eta a} \tag{11}$$

As the results, the average particle radius was evaluated to be 544 nm for the CB suspension after 3 h. This is consistent with the Z-setup result obtained using Eq. (7). Because of the crossover behavior originated from the diffusion and sedimentation terms in Eq. (10), the apparent exponent n for submicron particles can vary between 1 and 2 at the frequency accessible by the broadband transducer. Note that, for the submicron-sized particles, the particle size appeared in Eq. (11) can be solely determined by the diffusive part of Eq. (10) without priori information about C_y (the sedimentation part). If necessary, C_y can be further determined using Eq. (9) once D is estimated.

Fig. 4 shows the image profile of the scattered intensity obtained for the aqueous suspension of the CB particles in the presence of Nafion. Compared to the above aqueous suspension without Nafion, the image is fairly homogenous, and no large scatterer was found. The condition of the suspension was fairly stable over a long time period (at least 3 h). The double logarithmic plot of $\ln g^{(1)}(\tau)$ now indicated that the dynamics was governed by Brownian motion ($\ln g^{(1)}(\tau) \sim \langle r^2 \rangle \sim \tau^1$). The average particle radius was determined to be 344 nm by diffusive mode calculation,

$$g_y^{(1)}(t, \tau) = \exp(-Dq^2\tau) \tag{12}$$

This fact suggests that the Nafion is an effective dispersant for the CB suspension and suppresses the formation of large agglomerates.

So far, the effect of Nafion on the dispersibility of the CB suspension was studied for the CB suspensions. Similar experiments were carried out for a series of alcohol-rich suspensions. The results are summarized in Table 1. From the scattered intensity image, we found that there were extraordinarily large agglomerates passing through the scattering volume in the absence of Nafion (Fig. 2). The time-correlation function allowed us to evaluate the size of particles in homogeneous area of the image. As the results, noticeable submicron/micron-sized aggregates were found. On the contrary, from Fig. 4, Nafion was found to be an effective dispersant to suppress the formation of large agglomerate. Although complete settling of micron-sized aggregates was confirmed and the supernatant solution was analyzed, the size of Brownian particle was still 344 nm, which must be an assembly of small primary nanoparticles. In contrast to the case of the water-rich CB suspensions, the alcohol rich suspension showed a broader size distribution even in the presence of Nafion. On the other hand, it was found that the alcohol-rich suspension contained a smaller structure of CB. But, the particle radius was still in the submicron regime.

Therefore, we attempted to find primary nanoparticles in aqueous suspension with an aid of phosphotungustic acid (PWA), a superacid, as a stabilizer. Since PWA has a unique effect to stabilize the surface of CB by attaching the large anion to the surface, the large CB aggregates are expected to fragment into smaller pieces and finally reach nanometer-size [7]. Prescribed amount of CB was mixed with a 10 mM aqueous solution of PWA to obtain 1 wt% CB solution, followed by sonication for 3 h. The remaining large aggregates were centrifuged, and the supernatant solution was investigated as the sample. After the experiments, the CB concentration was determined to be 0.1 wt%. Fig. 5 shows the time-correlation function of the CB suspension prepared by decomposition of CB powder with PWA. As shown in the figure, the time-correlation function showed the pure diffusion mode, and the size of the particle was evaluated to be 31.4 nm.

As shown above, the CB particles easily form large agglomerates in the absence of Nafion, and they were observed at the onset of sedimentation. On the other hand, Nafion and/or PWA have a role to suppress formation of large agglomerates. The evaluated particle diameter became fairly small compared to the CB suspension without Nafion. Fig. 6 shows the average particle diameter, d, obtained for the

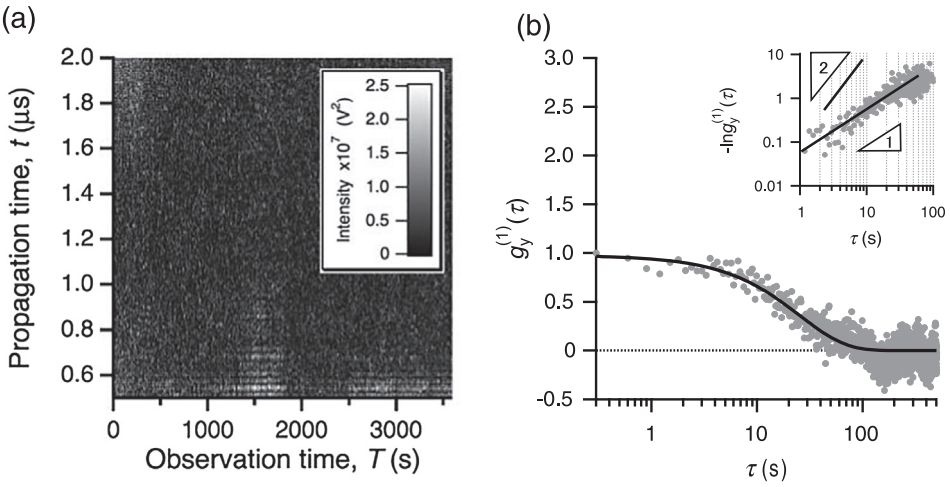

Fig. 4. The image profile of the scattered intensity obtained for the aqueous suspension of CB particle in the presence of Nafion. (b) The corresponding time correlation function.

Table 1
Summary of the particle size evaluated by the FD-DSS technique.

Sample	Polymer dispersant	Particle radius		
		Primary particle[a]	Aggregate[a]	Agglomerate[b]
Water-rich	N.A.		503 nm (544 nm)	0.4–2 μm
	Nafion		344 nm	
Alcohol-rich	N.A.		220 nm	1.5–2.15 μm
	Nafion		215 nm	711 nm
PWA aq.	Nafion	31.4 nm		

[a] Determined from the time-correlation function obtained for the supernatant solution.
[b] Determined from the intensity map or time-correlation function of the original suspension.

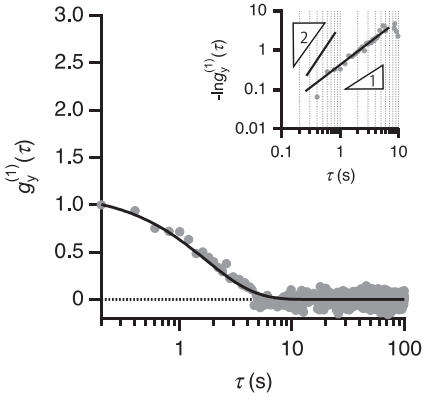

Fig. 5. The time-correlation function of the CB suspension prepared by decomposition of CB power in the presence of PWA under sonication.

CB/PWA suspension as a function of the CB concentration. The open and close circles respectively show the data obtained for the suspension with and without Nafion. For the micron-sized particles, the diameter was evaluated by the vertical setup with Eq. (7). As the particle size becomes smaller, undershooting of the correlation function (contribution from the cosine term) is less prominent, leading to uncertainty of evaluation of the sedimentation velocity. Therefore, the horizontal setup was also employed to evaluate the particle size from the time-correlation function consisting of both the sedimentation and diffusion

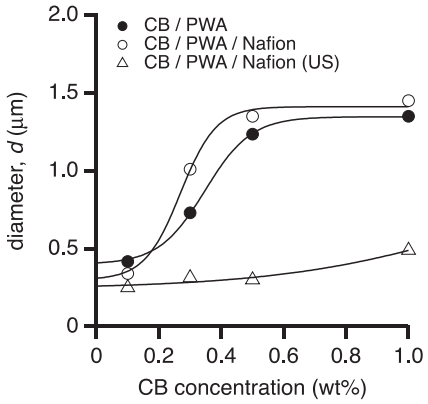

Fig. 6. CB concentration dependence of size of aggregation in suspension in the presence and absence of Nafion.

terms, i.e., from crossover fitting with Eq. (10). Note that, in general, the vertical and horizontal analysis give the equivalent result. From the FD-DSS analysis, it was found that the d obtained for the CB/PWA suspension exhibited similar CB concentration dependence irrespective of the presence of Nafion.

Localization of the dispersant at the surface of CB particle is an important subject to characterize the CB suspensions. Subsequently, we carried out ultrasonic spectroscopy (US) analysis to understand the structure of CB particles in suspension. In our previous paper, we showed that US was a useful technique to determine the particle size as well as the elasticity of individual particle dispersed in liquid without dilution of the sample [18,32,43–45]. The technique was employed to examine the structure of the CB particles in-situ. Fig. 7(a) and (b) respectively show the attenuation coefficient α and the phase velocity c obtained for the CB/PWA suspension without Nafion. Owing to the presence of PWA, no agglomerate was found in spite of the absence of Nafion. Increase in α and c with the CB concentration was observed regardless of the frequency range studied here. The solid lines indicate the theoretical prediction reproduced by the scattering function theory combined with the dispersion relation. Since the thermal contribution was expected to be sufficiently weak, the scattering matrix was calculated by the four equations in terms of the radial pressure, radial displacement, tangential pressure and tangential displacement, so called the ECAH44 model [32]. In order to ensure the discussion based on the US spectra, it is preferable to minimize the adjustable parameters. To evaluate the plausible particle size distribution, its average value was taken from the FD-DSS data, and was fixed throughout the US analysis.

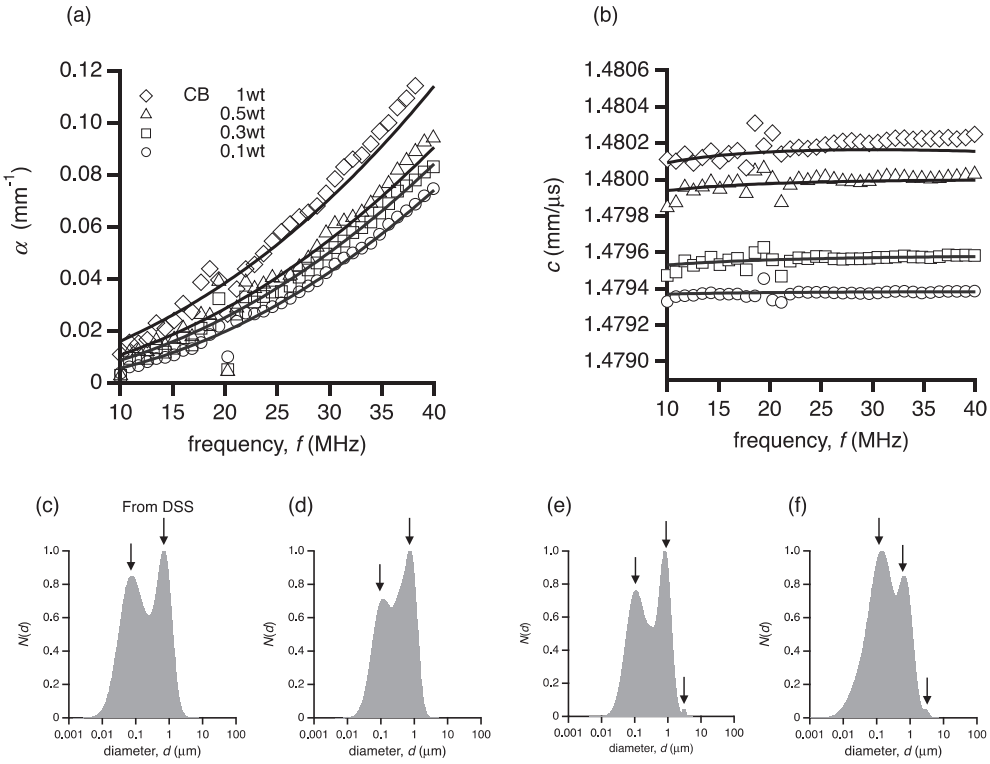

Fig. 7. Frequency dependence of (a) the attenuation coefficient and (b) phase velocity obtained for the CB/PWA suspension with different particle concentrations. Particle size distribution evaluated by the US analysis for the CB concentration (c) 0.1, (d) 0.3, (e) 0.5, and (f) 1 wt%.

For a suspension having aggregates and/or agglomerates, the average size of the individual structure was employed as the peak location as well. (the arrows in Figure (c)–(f)). Then, the adjustable parameters are the width and the height of the peaks in the analysis. The evaluated size distributions are shown in Fig. 7(c)–(f). The details of the calculation will be explained later.

Fig. 8(a) and (b) respectively show the attenuation coefficient α and the phase velocity c obtained for the CB/PWA suspension with Nafion. In contrast to the CB/PWA suspension, the CB/PWA/Nafion suspension exhibited different CB concentration dependence in terms of c. The theoretical interpretation of the results represented by the solid lines will be given below.

Before describing the detail of analysis, let us show the CB concentration dependence of α at a fixed frequency, 30 MHz, in Fig. 9(a). First, α obtained for the CB/PWA/Nafion suspension (open circles) was larger than that without Nafion (closed circles). This is mainly due to the intrinsic absorption of Nafion. However, α obtained for the CB/PWA suspension showed stronger CB concentration dependence than the CB/PWA/Nafion suspension as realized from the difference of the attenuation coefficient between the CB suspension and the reference solution as shown in the inset. This suggests that growth of rigid aggregates is more prominent for the CB/PWA suspension without Nafion than the CB/PWA/Nafion suspension, and the actual cluster size for the latter may be smaller. As shown in Fig. 6, the average particle size evaluated by the FD-DSS method was almost the same, or even larger for the suspension with Nafion. Therefore, it would be interesting to reconsider the physical meaning of the results obtained by the FD-DSS and US techniques.

Fig. 9(b) shows the CB concentration dependence of c obtained for the CB/PWA suspension with and without Nafion at 30 MHz. In contrast to α, the CB concentration dependence of c obtained for the CB/PWA suspension without Nafion was different from that with Nafion. For the CB/PWA suspension, c increased with the CB concentration, and became closer to the value of PWA aqueous solution ($c_{\mathrm{PWAaq}} = 1.47813$ mm/μs) and distilled water ($c_{\mathrm{water}} = 1.49673$ mm/μs). In general, as solid scatterers are present in the system, the frequency dependence of c would shift to the lower frequency with increasing the particle size, and to the higher frequency with increasing the elasticity of particle. And also, the larger and softer particles exhibit the smaller c at a fixed frequency and fixed volume fraction. From the FD-DSS results of Fig. 6, it was found that increase in the CB concentration led to formation of larger aggregates. Therefore, increase in c for the CB/PWA suspension cannot be explained by the decrease in the particle size. In addition, elasticity of the aggregates would be the same, or even softer as weakly bonded agglomerates are formed. If this is the case, c could decrease with the CB concentration. Thus, changes in the particle size and the elasticity could not be responsible for the increase in c. From all considerations, we propose here that the increase in c is due to change in the property of surround liquid. For example, if PWA is attracted at the surface of CB, the effective concentration of PWA in aqueous phase will decrease with the CB concentration. Similar finding was reported previously [7]. This would explain the increase in c with the CB concentration for the CB/PWA suspension.

The problem of the US analysis is the number of adjustable parameters in the analysis. In this particular case, the longitudinal velocity for liquid phase, c_{L1}, the longitudinal velocity for particle, c_{L2}, the shear velocity of particle, c_{S2}, and the particle size distribution are unknown variables, which dominate the US spectra. Note that the density was determined by an independent experiment prior to the US analysis, and it was found to be $\rho = 1.84$ (g/cm^3). Other parameters obtained by the analysis are listed in Table 2. As described above, increase in c for the CB/PWA suspension is mainly ascribed to the change in the longitudinal velocity of the surrounding liquid. Therefore, the vertical shift of c was adjusted by changing c_{L1} first, followed by estimation of c_{L2} and c_{S2} to obtain the best-fit results. Note that we have difficulty to simultaneously determine c_{L2} and c_{S2} because the fitting is insensitive to these parameters. Therefore, these results contain uncertainty to conclude the quantitative elastic parameters of the CB aggregates.

Similar analysis was performed for the CB/PWA suspension in the presence of Nafion as shown in Fig. 8. However, no relevant parameter

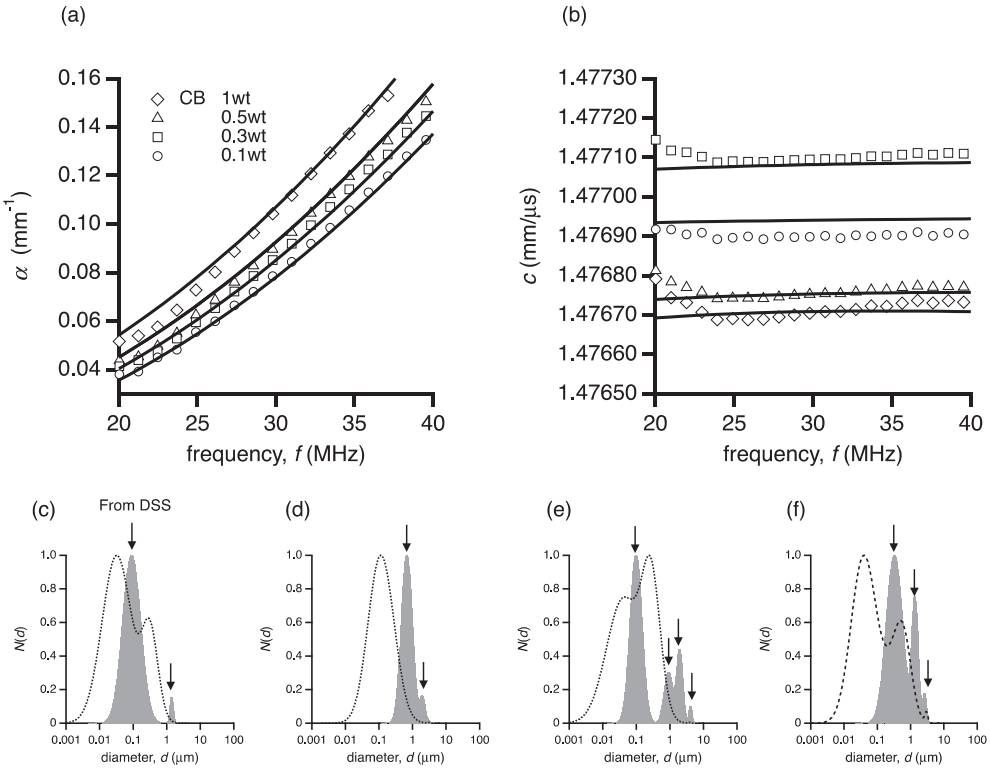

Fig. 8. Frequency dependence of (a) the attenuation coefficient and (b) phase velocity obtained for the CB/PWA/Nafion suspension with different particle concentrations. Particle size distribution evaluated by the US analysis for the CB concentration (c) 0.1, (d) 0.3, (e) 0.5, and (f) 1 wt%.

was found as the longitudinal and shear velocity of the CB particle in the CB/PWA/Nafion suspensions using the particle size distribution evaluated by the FD-DSS data. Therefore, the peak position was also changed to fit the experimental data. As the result, it was found that the particle size evaluated by the US analysis was smaller than that obtained by the FD-DSS analysis. From the FD-DSS method, the hydrodynamic radius can be evaluated via the time-dependence of particle motion, whereas the US method givens information on the elastic properties of particle by probing the propagation of the acoustic waves with a mechanical contrast. Therefore, in the US technique, unless the clusters are sufficiently bonded to allow propagation of the displacement, the individual small particles rather than the assembly of particles could be observed. On the other hand, the FD-DSS technique probes the effective diameter of large CB/Nafion clusters. Although it was not shown here, the hydrodynamic radius significantly increased with the Nafion concentration. Since it is difficult to envisage that Nafion leads to formation of large agglomerates, this also supports the FD-DSS

Table 2
The results of the US analysis for the CB/PWA suspensions without Nafion.

CB concentration (wt %)		c_{L1} (mm/μs)	c_{L2} (mm/μs)	c_{S2} (mm/μs)	α_2/f^2 (s^2/m)	ρ (g/cm^3)
CB/PWA	0.1	1.47940	2.2	1.25	2×10^{-12}	1.84
	0.3	1.47955	2.2	1.15	2×10^{-12}	1.84
	0.5	1.47980	2.2	0.95	2×10^{-12}	1.84
	1.0	1.47985	2.2	0.95	2×10^{-12}	1.84

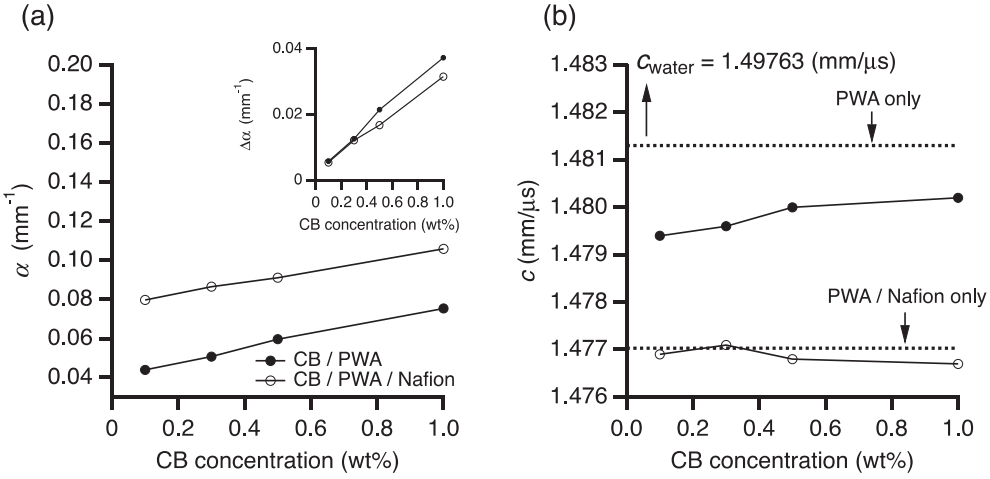

Fig. 9. CB concentration dependence of (a) the attenuation coefficient and (b) phase velocity obtained for the CB/PWA and CB/PWA/Nafion suspensions with different particle concentrations. The inset in Figure (a) shows the excess absorption, Δα obtained for the CB/PWA suspensions with and without Nafion.

Table 3
The results of the US analysis for the CB/PWA suspensions with Nafion.

CB concentration (wt %)		c_{L1} (mm/μs)	c_{L2} (mm/μs)	c_{S2} (mm/μs)	α_2/f^2 (s^2/m)	ρ (g/cm^3)
CB/PWA/Nafion	0.1	1.47703	1.95	1.18	2×10^{-12}	1.84
	0.3	1.47703	2.35	1.20	2×10^{-12}	1.84
	0.5	1.47703	2.00	1.17	2×10^{-12}	1.84
	1.0	1.47703	2.06	1.20	2×10^{-12}	1.84

results providing the larger particle size. In Fig. 9(a), we showed that the attenuation coefficient exhibited the weaker CB concentration dependence. This also suggests that coalesce of the CB aggregates is less prominent for the CB/PWA/Nafion system, and the actual particle size would be smaller than hydrodynamic radius evaluated by the FD-DSS technique.

From Fig. 9(b), we observed decrease in the phase velocity of the CB/PWA suspensions. This could be explained by the increase in the size of the scatterers as straightforward. On the contrary, c could decrease with decreasing the stiffness of the cluster. However, d was smaller than 1.5 μm for all the CB concentrations. In addition, with increasing the CB concentration, c obtained for the CB/PWA/Nafion suspension deviated from those of aqueous solution of PWA/Nafion. Since they also deviated from those of PWA aqueous solution and distilled water, localization of the Nafion on the surface of the CB particles unlikely occurred. As described above, increase in the cluster size could lead to decrease in c. Therefore, it is suggested that as a possible structural model for the CB/PWA/Nafion system, Nafion could be dispersed homogenously in the suspension to prevent formation of large aggregates and agglomerates, and the CB/PWA clusters could disperse with Nafion as a binder.

The evaluated particle size was depicted in Fig. 8(c)–(f) by the dashed lines and Fig. 6 as the triangle markers. The other parameters determined by the analysis are shown in Table 3. In contrast to the case of the CB/PWA suspensions without Nafion, the longitudinal velocity of the surrounding liquid, $c_{L1} = 1.47703$ mm/μs, was found to be constant. While we tried to find a possibility to vary c_{L1} with the CB concentration, the fitted parameter rather decreased with the CB concentration, which was obviously unphysical since $c_{L1} = 1.4813$ mm/μs for the pure aqueous solution of PWA was larger than that for the CB/PWA with Nafion. Therefore, $c_{L1} = 1.47703$ mm/μs was fixed throughout the US analysis of CB/PWA/Nafion.

In this study, we showed that the frequency-domain dynamic ultrasound scattering technique (FD-DSS) could be a promising tool to investigate the dynamics as well as the particle size having hierarchal structures of carbon black. In other words, evaluation of the suspension containing primary nanoparticles, secondary aggregates, and ternary agglomerates is possible. On the other hand, we did not evaluate the aspect ratio [46] which was also very important characteristics of CB aggregates and agglomerates. Although, at present, the FD-DSS analysis offers only the equivalent spherical radius (hydrodynamic radius), an elaborate scattering function analysis would allow us to carry out more detailed evaluation of the structures in the future.

5. Conclusions

The frequency-domain dynamic ultrasound scattering method (FD-DSS) is a promising technique to analyze the motion and the size of particles in suspension in range several tens of nanometers to several hundreds of micrometers. The striking advantage is that FD-DSS enables us to distinguish the type of particle motions, such as Brownian motion of nanoparticles and sedimentation of large aggregates. In this study, the technique was utilized to observe primary particle, secondary aggregate and ternary agglomerate of carbon black (CB) particles. Nafion was found to be an effective dispersant to suppress formation of large agglomerates, as can be seen from the intensity-field image of ultrasound scattering. Alcohol-rich system showed better characteristics in terms of the size of aggregates, but most of the particle size remained in the submicron regime. Nafion also works as a good dispersant in water rich system although the particle size was not so small as the alcohol-rich system. Despite the effort to obtain well-dispersed CB suspension both in alcohol and water with Nafion under sonication, the particles sizes were still in the submicron regime. Then, phosphotungstic acid was employed to obtain the CB nanoparticles. As the results, the CB particles with ca. 30 nm could be obtained by the dynamic ultrasound scattering technique. The possible structures of CB/PWA and CB/PWA/Nafion suspensions were discussed. For the CB/PWA suspension, thanks to the presence of Nafion, there was almost no agglomerate in the system. With increasing the CB concentration, the size of the CB aggregates increased. From the combinatorial analysis of the FD-DSS and the US technique, it was suggested that PWA was localized at the surface of the CB particles. On the contrary, the CB/PWA/Nafion suspension has better dispersibility in terms of suppression of formation of the CB aggregates. Nafion could be localized at the surface of the CB particle, but this was not the case for our CB/PWA/Nafion suspensions since PWA also played an effective role to stabilize the suspension. It was concluded that the ultrasonic scattering techniques could be very useful to evaluate the rigidity, the structure as well as the particle size ranging from nanometer to micrometer in suspension, which was difficult to be observed by conventional optical techniques.

Acknowledgements

This work was supported by KAKENHI (Grant-in-Aid for Scientific Research), No. 15K05627 from the Ministry of Education, Science, Sports, Culture, and Technology.

References

[1] F. Nsiba, N. Ayeda, Y. Yves, Chevalierb, Selection of dispersants for the dispersion of carbon black in organic medium, Prog. Org. Coat. 55 (2006) 303–310.
[2] L.B. Tunnicliffe, Flocculation and viscoelastic behaviour in carbon black-filled natural rubber, Macromol. Mater. Eng. 299 (2014) 1474–1483.
[3] S.K. Sharma, B.G. Pollet, Support materials for PEMFC and DMFC electrocatalysts—A review, J. Power Sources 208 (2012) 96–119.
[4] A. Galvez, N. Herlin-Boime, C. Reynaud, C. Clinard, J.-N. Clinard, Carbon nanoparticles from laser pyrolysis, Carbon 40 (2002) 2775–2789.
[5] J. Jang, J.H. Oh, G.D. Stucky, Fabrication of ultrafine conducting polymer and graphite nanoparticles, Angew. Chem. Int. Ed. 41 (2002) 4016–4019.
[6] W.K. Hsu, M. Terrones, J.P. Hare, H. Terrones, H.W. Kroto, D.R.M. Walton, Electrolytic formation of carbon nanostructures, Chem. Phys. Lett. 262 (1996) 161–166.
[7] P. Garrigue, M.-H. Delville, C. Labrugère, E. Cloutet, P.J. Kulesza, J.P. Morand, A. Kuhn, Top–down approach for the preparation of colloidal carbon nanoparticles, Chem. Mater. 16 (2004) 2984–2986.
[8] J.-H. Lin, H.-W. Chen, K.-T. Wangb, F.-H. Liaw, A novel method for grafting polymers on carbon blacks, J. Mater. Chem 8 (1998) 2169–2173.
[9] T. Liu, S. Jia, T. Kowalewski, K. Matyjaszewski, R. Casado-Portilla, J. Belmont, Water-dispersible carbon black nanocomposites prepared by surface-initiated atom transfer radical polymerization in protic media, Macromolecules 39 (2006) 548–556.
[10] Y. Hanada, S. Masuda, M. Iijima, H. Kamiya, Analysis of dispersion and aggregation behavior of carbon black particles in aqueous suspension by colloid probe AFM method, Adv. Powder. Technol. 24 (2013) 844–851.
[11] S. Lu, D.D.L. Chung, Viscoelastic behavior of carbon black and its relationship with the aggregate size, Carbon 60 (2013) 346–355.
[12] H. Parant, G. Muller, T. Le Mercier, J.M. Tarascon, P. Poulin, A. Colin, Flowing suspensions of carbon black with high electronic conductivity for flow applications: comparison between carbons black and exhibition of specific aggregation of carbon particles, Carbon 119 (2017) 10–20.
[13] C. Jäger, T. Henning, R. Schlögl, O. Spillecke, Spectral properties of carbon black, J. Non-Cryst. Solids 258 (1999) 161–179.
[14] Z.C. Kang, Z.L. Wang, On accretion of nanosize carbon spheres, J. Phys. Chem. 100 (1996) 5163–5165.
[15] J. Lahaye, F. Ehrburger-Dolle, Mechanisms of carbon black formation. Correlation with the morphology of aggregates, Carbon 32 (1994) 1319–1324.
[16] L. Levy, I.S. Chaudhuri, N. Krueger, R.J. McCunney, Does carbon black disaggregate in lung fluid? A critical assessment, Chem. Res. Toxicol. 25 (2012) 2001–2006.
[17] R. Xu, C. Wu, H. Xu, Particle size and zeta potential of carbon black in liquid media, Carbon 45 (2007) 2806–2809.

[18] T. Norisuye, Structures and dynamics of microparticles in suspension studied using ultrasound scattering techniques, Polym. Int. 66 (2017) 175–186.
[19] M.L. Cowan, J.H. Page, D.A. Weitz, Velocity fluctuations in fluidized suspensions probed by ultrasonic correlation spectroscopy, Phys. Rev. Lett. 85 (2000) 453–456.
[20] K. Kobayashi, T. Norisuye, K. Sugita, H. Nakanishi, Q. Tran-Cong-Miyata, Dynamics of nanometer- and micrometer-sized particles in suspension probed by dynamic ultrasound scattering techniques, J. Appl. Phys. 122 (2017) 045106 045108p.
[21] A. Nagao, M. Kohyama, T. Norisuye, Q. Tran-Cong-Miyata, Simultaneous observation and analysis of sedimentation and floating motions of microspheres investigated by phase mode-dynamic ultrasound scattering, J. Appl. Phys. 105 (2009) 023526.
[22] A. Nagao, T. Norisuye, M. Kohyama, T. Yawada, Q. Tran-Cong-Miyata, Collective motion of microspheres in suspensions observed by phase-mode dynamic ultrasound scattering technique, Ultrasonics 52 (2012) 628–635.
[23] K. Igarashi, T. Norisuye, K. Kobayashi, K. Sugita, H. Nakanishi, Q. Tran-Cong-Miyata, Dynamics of submicron microsphere suspensions observed by dynamic ultrasound scattering techniques in the frequency-domain, J. Appl. Phys. 115 (2014) 203506.
[24] G. Wu, S. Asai, M. Sumita, T. Hattori, R. Higuchi, J. Washiyama, Estimation of flocculation structure in filled polymer composites by dynamic rheological measurements, Colloid Polym. Sci. 278 (2000) 220–228.
[25] A.I. Medalia, E. Hagopian, Rheology of dispersant-free aqueous slurries of carbon black, Rheol. Acta 3 (1963) 100–111.
[26] T. Konno, T. Norisuye, K. Sugita, H. Nakanishi, Q. Tran-Cong-Miyata, Dynamics of micron-sized particles in dilute and concentrated suspensions probed by dynamic ultrasound scattering techniques, Ultrasonics 65 (2016) 59–68.
[27] T. Sawada, T. Norisuye, M. Kohyama, K. Sugita, H. Nakanishi, Q. Tran-Cong-Miyata, Effects of pulse repetition rate and incident beam energy on the dynamic ultrasound scattering data, Jpn. J. Appl. Phys. 53 (2014) 07KC10.
[28] T. Norisuye, S. Sasa, K. Takeda, M. Kohyama, Q. Tran-Cong-Miyata, Simultaneous evaluation of ultrasound velocity, attenuation and density of polymer solutions observed by multi-echo ultrasound spectroscopy, Ultrasonics 51 (2011) 215–222.
[29] P.C. Waterman, R. Truell, Multiple scattering of waves, J. Math. Phys. (N.Y.) 2 (1961) 512–537.
[30] L.L. Foldy, The multiple scattering of waves. I. General theory of isotropic scattering by randomly distributed scatterers, Phys. Rev. 67 (1945) 107–119.
[31] P. Lloyd, M.V. Berry, Wave propagation through an assembly of spheres Iv. Relations between different multiple scattering theories, Proc. Phys. Soc. 91 (1967) 678–688.
[32] H. Mori, T. Norisuye, H. Nakanishi, Q. Tran-Cong-Miyata, Ultrasound attenuation and phase velocity of micrometer-sized particle suspensions with viscous and thermal losses, Ultrasonics 83 (2018) 171–178.
[33] P. Epstein, R.R. Carhart, The absorption of sound in suspensions and emulsions. I. Water fog in air, J. Acoust. Soc. Am. 25 (1953) 553–565.
[34] J.R. Allegra, S.A. Hawley, Attenuation of sound in suspensions and emulsions: theory and experiments, J. Acoust. Soc. Am. 51 (1972) 1545–1564.
[35] R.E. Challis, M.J.W. Povey, M.L. Mather, A.K. Holmes, Ultrasound techniques for characterizing colloidal dispersions, Rep. Prog. Phys. 68 (2005) 1541–1637.
[36] R.E. Challis, J.S. Tebbutt, A.K. Holmes, Equivalence between three scattering formulations for ultrasonic wave propagation in particulate mixtures, J. Phys. D-Appl. Phys. 31 (1998) 3481–3497.
[37] J.F. Richardson, W.N. Zaki, Sedimentation and fluidisation: part I, Chem. Eng. Res. Des. 32 (1954) 35–53.
[38] M. Kohyama, T. Norisuye, Q. Tran-Cong-Miyata, Dynamics of microsphere suspensions probed by high frequency dynamic ultrasound scattering, Macromolecules 42 (2009) 752–759.
[39] R.E. Caflisch, J.H.C. Luke, Variance in the sedimentation speed of a suspension, Phys. Fluids 28 (1985) 759–760.
[40] M.P. Brenner, Screening mechanisms in sedimentation, Phys. Fluids 11 (1999) 754–772.
[41] P.J. Mucha, S.Y. Tee, D.A. Weitz, B.I. Shraiman, M.P. Brenner, A model for velocity fluctuations in sedimentation, J. Fluid Mech. 501 (2004) 71–104.
[42] É. Guazzelli, J. Hinch, Fluctuations and instability in sedimentation, Annu. Rev. Fluid Mech. 43 (2011) 97–116.
[43] K. Kubo, T. Norisuye, T.N. Tran, D. Shibata, H. Nakanishi, Q. Tran-Cong-Miyata, Sound velocity and attenuation coefficient of hard and hollow microparticle suspensions observed by ultrasound spectroscopy, Ultrasonics 62 (2015) 186–194.
[44] T.N. Tran, T. Norisuye, D. Shibata, H. Nakanishi, Q. Tran-Cong-Miyata, Determination of particle size distribution and elastic properties of silica microcapsules by ultrasound spectroscopy, Jpn. J. Appl. Phys. 55 (2016) 07KC01.
[45] T. Inoue, T. Norisuye, K. Sugita, H. Nakanishi, Q. Tran-Cong-Miyata, Size distribution and elastic properties of thermo-responsive polymer gel micro-particles in suspension probed by ultrasonic spectroscopy, Ultrasonics 82 (2018) 31–38.
[46] E.A. Grulke, S.B. Rice, J. Xiong, K. Yamamoto, T.H. Yoon, K. Thomson, M. Saffaripour, G.J. Smallwood, J.W. Lambert, A.J. Stromberg, R. Macy, N.J. Briot, D. Qian, Size and shape distributions of carbon black aggregates by transmission electron microscopy, Carbon 130 (2018) 822–833.